Magnetic Resonance in Medicine 51:655–660 (2004)

Real-Time Cardiac MRI at 3 Tesla

Krishna S. Nayak,[1,2*] Charles H. Cunningham,[1] Juan M. Santos,[1] and John M. Pauly[1]

Real-time cardiac and coronary MRI at 1.5T is relatively "signal starved" and the 3T platform is attractive for its immediate factor of two increase in magnetization. Cardiac imaging at 3T, however, is both subtly and significantly different from imaging at 1.5T because of increased susceptibility artifacts, differences in tissue relaxation, and RF homogeneity issues. New RF excitation and pulse sequence designs are presented which deal with the fat-suppression requirements and off-resonance issues at 3T. Real-time cardiac imaging at 3T is demonstrated with high blood SNR, blood-myocardium CNR, resolution, and image quality, using new spectral-spatial RF pulses and fast spiral gradient echo pulse sequences. The proposed sequence achieves 1.5 mm in-plane resolution over a 20 cm FOV, with a 5.52 mm measured slice thickness and 32 dB of lipid suppression. Complete images are acquired every 120 ms and are reconstructed and displayed at 24 frames/sec using a sliding window. Results from healthy volunteers show improved image quality, a 53% improvement in blood SNR efficiency, and a 232% improvement in blood-myocardium CNR efficiency compared to 1.5T. Magn Reson Med 51:655–660, 2004.

Key words: real-time MRI; high field; cardiac imaging; spirals; spectral-spatial excitation

Real-time cardiac MRI at 1.5T has proved to be clinically useful for evaluating cardiac function, visualizing cardiac flow, and localizing scan planes for coronary imaging (1–6). It has also shown promise as a valuable foundation for multifaceted cardiac MR examinations. In general, real-time imaging pushes the limits of temporal and spatial resolution, as constrained by signal-to-noise ratio (SNR). This is especially true for real-time coronary imaging (7), which is an application emphasized in this article, and which requires high spatial and temporal resolution and borders on inadequate SNR.

High field imaging is attractive because it has the potential to significantly improve SNR due to increased polarization of spins. With novel pulse sequence design, this SNR boost can be used to improve spatial resolution and/or temporal resolution. The advent of clinical 3T scanning has motivated our group to develop real-time cardiac imaging at 3T and to find ways to exploit this increase in magnetization while managing the effects of increased susceptibility off-resonance, longer T_1s, and RF inhomogeneity. At 3T, susceptibility effects are expected to produce up to ±130 Hz of off-resonance over the heart, with focal areas towards the lungs and near large draining veins (8,9). T_1s are expected to be roughly 1550 ms for blood and 1115 ms for myocardium (8). Finally, the transmitted B_1 field can be highly inhomogeneous and body size-dependent (10), and RF power deposition (or SAR) is another critical design constraint.

We present new optimized spiral gradient echo imaging sequences that achieve the necessary temporal resolution for real-time cardiac imaging and the necessary fat suppression and spatial resolution for real-time coronary imaging. New spectral-spatial RF pulses were designed to take advantage of the larger fat-water frequency difference (≈440 Hz), and short yet efficient spiral readouts mitigate off-resonance blurring artifacts. Simulation, phantom, and in vivo results are presented.

MATERIALS AND METHODS

Experiments were performed on a GE Signa 3T LX system and a GE Signa 1.5T LX system, both with gradients capable of 40 mT/m amplitudes and 150 T/m/s slew rates, and receivers supporting 4 μs sampling (±125 kHz). Body coils capable of peak B_1 of 16 μT (estimated for a large patient) were used for RF transmission, and 5-inch surface coils were used for signal reception in all studies. The institutional review board of Stanford University approved the imaging protocols. Each subject was screened for MRI risk factors and provided informed consent in accordance with institutional policy.

Off-Resonance

High-resolution field maps were acquired using a product multislice spiral sequence that covered 8 short-axis slices in two 16-sec breathholds. Acquired field maps were comparable in frequency range to those observed by Noeske et al. (8) (±130 Hz). Focal inhomogeneities near the lungs and near the posterior vein (PVLV) were observed. Figure 1 shows two slices from one such study. In this particular case we observed 130 Hz of off-resonance frequency shifts across the myocardium (not including focal areas), and 160 Hz of off-resonance across the extent of RCA visualized.

RF Design

The implementation of spectral-spatial RF pulses (11–13) for cardiac imaging at 3T presents a significant advantage vs. 1.5T: the doubling of the frequency difference between lipid and water implies that, in theory, it is possible to design pulses that are half the duration. Below, we describe our design of an exceptionally short (2.8 ms) spec-

[1]Magnetic Resonance Systems Research Laboratory, Department of Electrical Engineering, Stanford University, Stanford, California.

[2]Signal and Image Processing Institute, Department of Electrical Engineering, University of Southern California, Los Angeles, California.

Grant sponsors: National Institutes of Health, GE Medical Systems.

A preliminary account of this work was presented at the 11th annual meeting of the International Society for Magnetic Resonance in Medicine, Toronto, July 2003 (Late-Breaking MR Clinical Science Session).

*Correspondence to: Krishna S. Nayak, 3740 McClintock Ave, EEB 406, University of Southern California, Los Angeles, CA 90089-2564. E-mail: knayak@sipi.usc.edu

Received 2 September 2003; revised 19 November 2003; accepted 19 December 2003.

DOI 10.1002/mrm.20053
Published online in Wiley InterScience (www.interscience.wiley.com).

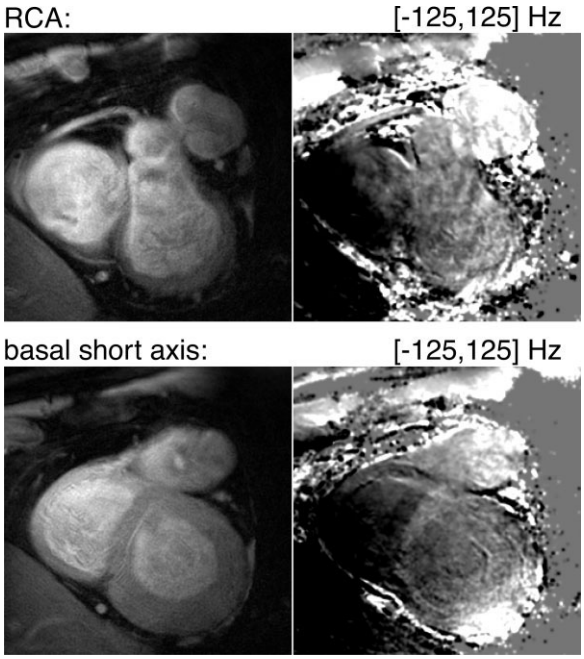

FIG. 1. Field maps acquired at 3T in a healthy volunteer. (Top) Right coronary view and (bottom) short axis view. On the left are images, and on the right are field maps with the range −125 to 125 Hz.

tral-spatial pulse for 3T, taking full advantage of the gradient and RF capabilities.

With the goal of making the spectral-spatial pulse as short as possible, we decided that the pulse would consist of just three sublobes, as this is the minimum number for which a reasonably flat null on the lipid resonance can be achieved. A "fly-back" design (14) was chosen (RF transmitted only during positive lobes of the oscillating gradient) to reduce motion-induced phase. When using nonflyback designs in the heart, we observed severe artifacts and signal voids from through-plane flow. For the spectral profile, defined by the envelope modulating the RF sublobes, the 1-2-1 binomial sequence was used. This is comparable but shorter than the 1-3-3-1 binomial sequence used by Schick (12). For the spatial profile, defined by the shape of each sublobe, a shape with time-bandwidth product of 3.5 was computed. The duration of each gradient sublobe was set to 560 μs so that the first spectral null is centered on lipid at −440 Hz, and the sublobe shape uses the full gradient capability (amplitude and slew rate). Lastly, the variable rate selective excitation (VERSE) algorithm (15) was applied to compensate for the fact that RF is transmitted while the gradient is changing. VERSE is a method for designing excitation pulses with time-varying gradients, which allowed us to generate the largest possible gradient area during each sublobe, enabling thin slices. RF and gradient waveforms are shown in Fig. 2. The simulated excitation profile shown in Fig. 3b was computed with a numerical Bloch-equation simulation using MATLAB (MathWorks, Natick, MA). Note that this pulse uses all of our hardware capability (gradient amplitude and slew rate, and peak B_1 for a 62° tip angle in a large patient).

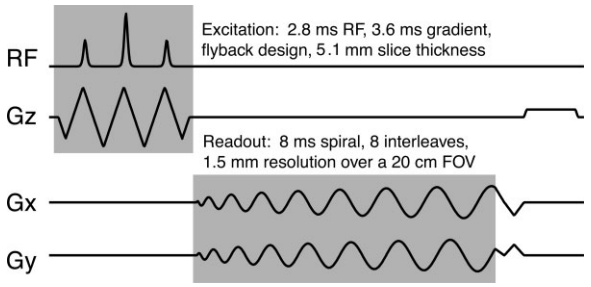

FIG. 2. Pulse sequence. 3.6 ms fly-back spectral-spatial excitation (2.8 ms RF), 8 ms spiral readouts, and 1 ms crusher. TE = 2 ms, TR = 15 ms, 8 interleaves, 120 ms per image, reconstructed and displayed at 24 frames/s.

Excitation Profile Measurement

The spectral-spatial excitation profile of the pulse was measured with a phantom experiment. A $1 \times 12 \times 12$ cm^3 block phantom was filled with distilled water doped with copper sulfate to achieve T_1 and T_2 of approximately 100 ms. A modified spin-echo pulse sequence was used. The spatial variation of the profile was resolved by phase encoding in the through-slice direction, and the spectral variation of the profile was resolved by applying a 0.61 mT/m gradient during excitation. A 256×256 encoding matrix was used, with an 8 cm FOV, TR/TE = 300/20 ms, and the body coil used for both excite and receive. The measured profile is shown in Fig. 3a.

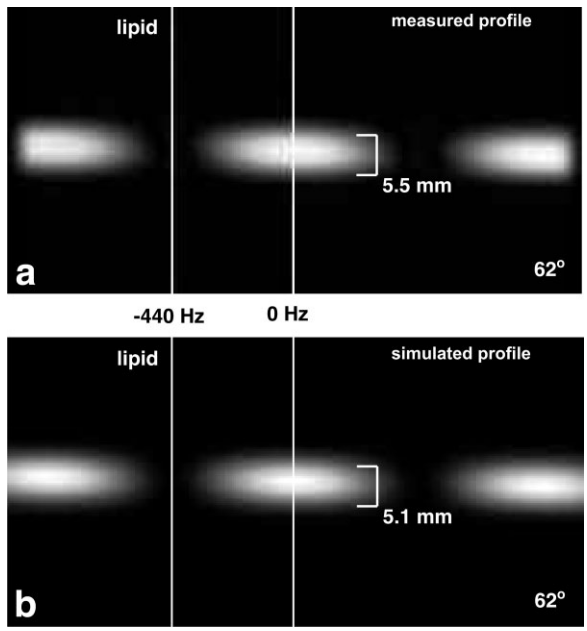

FIG. 3. Excitation profile for the spectral-spatial pulse. The (**a**) experimentally measured excitation profile, and (**b**) numerically computed profile both demonstrate the true null centered on lipid at −440 Hz. A measurement at the line through 0 Hz indicated a measured slice-thickness (width at half-maximum) of 5.52 mm. Based on the mean of pixels within ±20 Hz and ±0.25 mm from the null at −440 Hz, the pulse provides 32 dB of lipid suppression. Other than the difference in slice thickness, the measurement and simulation show excellent agreement.

It was noted that the slice profile achieved in practice was slightly thicker than that predicted by simulation. Because of the potential impact on the SNR comparison described below, this profile degradation was characterized. We eliminated simple timing and scaling errors in the pulse sequence and determined that the profile thickness scaled linearly with the inverse of gradient amplitude (over a range of 12–40 mT/m). To make an accurate measurement of the profile thickness, a conventional RF pulse with a constant gradient amplitude was used as a calibration, since we could be fairly sure that no gradient distortion was occurring with this pulse. With signal averaging used to get an SNR of 570, the minimum profile thickness was measured to be 5.52 mm; this is 8% larger than the 5.11 mm predicted by simulation.

The profile shown in Fig. 3a shows that the spectral-spatial pulse performs well despite its exceptionally short duration. Notice the true null at −440 Hz, the wide spectral passband of about 300 Hz, and the somewhat poor spatial profile (the gradient and RF constraints at 3T limit the slice profile and peak flip angle). The fact that fat can be left unexcited after just 2.8 ms of RF is possible because of the remarkably low time-bandwidth product of the pulse. From Fig. 3a this can be measured to be 1.5. This is a feature of the 1-2-1 amplitude variation of the subpulses.

Readout Design

Readouts were designed using established optimal spiral design techniques (16,17) based on our hardware. For the initial design, our goal was to keep the off-resonance artifact level comparable to what we experience at 1.5T. In spiral imaging, off-resonance blurring is roughly proportional to the amount of phase that accrues over each readout. Because susceptibility induced off-resonance is doubled at 3T, we shortened readouts by a factor of two to maintain the same phase over a readout. The 3T sequence used 8 ms spiral readouts shown in Fig. 2 (whereas 16 ms spiral readouts are typically used at 1.5T). This also represents a balance between shortening readouts to reduce off-resonance blurring and lengthening readouts to improve scan efficiency.

Because the excitations and readouts are half as long at 3T compared to 1.5T, this design effectively maintains the same readout duty cycle and can use double the number of spiral interleaves to achieve the same spatial and temporal resolution. Comparable scan parameters at 1.5T and 3T are summarized in Table 1.

Real-Time Imaging

A custom communication and real-time reconstruction and display framework was used to control the scanner and view images in real time (18). The control computer was a dual-processor 2.4 GHz Athlon workstation running Linux. This was located adjacent to the scanner and was connected by Ethernet. The graphical user interface was written using the Qt toolkit (Trolltech.com), and reconstruction used fast gridding (19,20) and FFT (FFTW.org) routines.

During the design iteration process, we varied several parameters of the spiral gradient echo pulse sequence. A series of spectral-spatial excitation pulses were designed and tested, with and without fly-back flow compensation, with subpulses having time-bandwidth products of 2 to 8 (producing broad or sharp spatial profiles), and with 3 to 8 sublobes (producing broad or sharp spectral profiles). Spiral readouts of 3, 4, 6, 8, 12, and 16 ms duration were also used to achieve 1.5 mm resolution with different numbers of interleaves. The sequence finally used, which is shown in Fig. 2, and is described above, achieved 1.5 mm in-plane resolution over a 20-cm FOV, every 120 ms (8 interleaves with a 15 ms TR). Images were reconstructed and displayed at 24 frames/s using a sliding window. In sliding window reconstruction (21), interleaves are acquired continuously and images are reconstructed using the most recent set of interleaves that can produce a complete image.

Table 1
Scan Parameters at 1.5T and 3T

Parameter	1.5T	3T
Spectral-spatial excitation		
Duration	7.0 ms	3.6 ms
Slice thickness	5.52 mm	5.52 mm
Spiral readouts		
Duration	16.384 ms	8.192 ms
Interleaves	4	8
Resolution	1.5 mm	1.5 mm
TR (repetition time)	28 ms	15 ms
Tip angle	30–40°	25–30°
Time per image	112 ms	120 ms

During scanning, whenever the imaging slice is changed, a new field map is acquired (using the phase difference between two low-resolution images with different echo times) (1), and the transmit center frequency and linear shims are updated automatically. Due to increased off-resonance at 3T, it became necessary to shift the excitation center frequency on a per-slice basis by as much as 150 Hz during real-time scanning to prevent nonlipid areas from falling in the excitation stop-band.

SNR Comparison

The improvement in SNR as compared with real-time scanning at 1.5T was investigated in a series of experiments with normal volunteers. The parameters that held constant at the two field strengths were receive coil type and size (5-inch surface coil), net signal sampling time (64 ms), and spatial resolution ($1.5 \times 1.5 \times 5.52$ mm^3). Exactly the same slice profile was achieved at the two field strengths by using the same RF pulse as shown in Fig. 2, except stretched to twice the duration for the 1.5T experiment. The profile thickness was calibrated on the 1.5T scanner, as described above for the 3T system. Because of the spoilers at the end of each TR, as well as other overhead, the time-per-image was slightly shorter at 1.5T (112 ms) vs. 3T (120 ms).

For comparing SNR, axial images were used because the distortions in excitation profile had been characterized for the z-axis gradient coil, so we could be certain of the exact profile thickness in this orientation. Signal level was computed from a single time-frame by averaging the pixels in

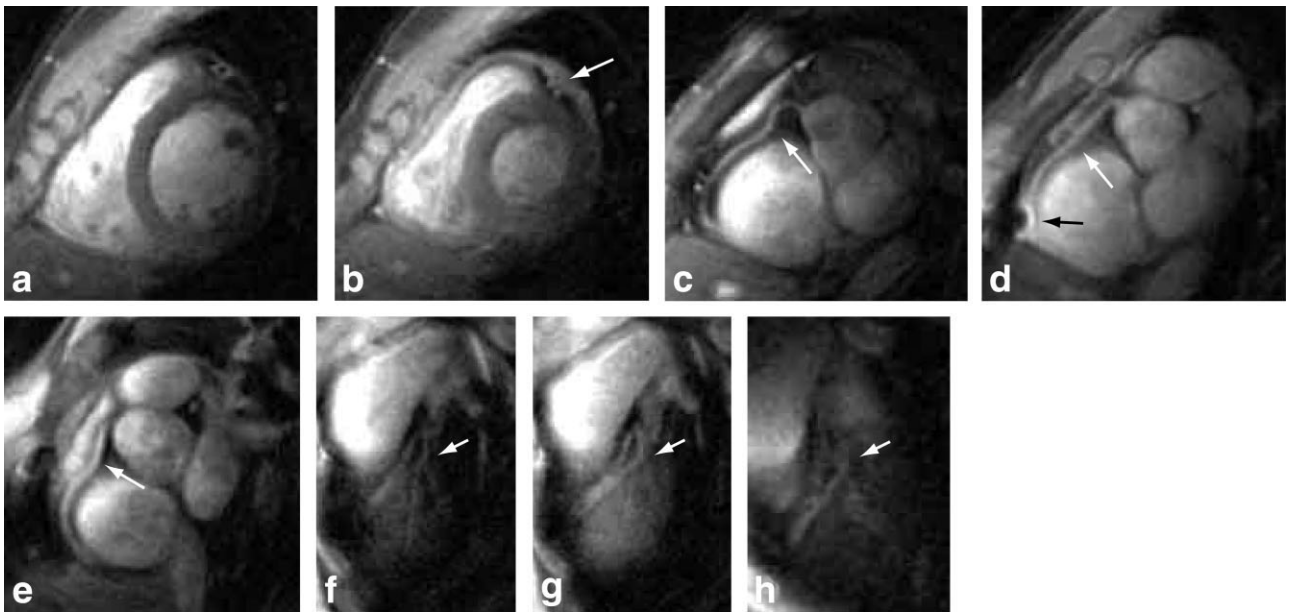

FIG. 4. Real-time cardiac images acquired at 3T. **a**: short-axis in diastole and (**b**) short-axis in systole in the same volunteer, (**c**, **d**) right coronary arteries in systole, (**e**) right coronary artery in diastole, (**f**, **g**) left coronary tree in two temporal frames from the same volunteer, and (**h**) left coronary tree in another volunteer. White arrows point at coronaries and a black arrow points at susceptibility artifact. Note the high SNR and quality of fat suppression in all views.

a region of interest in the left ventricle in mid-systole, which was intended to give signal from blood under similar conditions as in real-time imaging of the coronary arteries (in-flow enhancement, full oxygenation, etc.). Noise levels were computed by taking the standard deviation in images acquired immediately after the left-ventricle images, but with the RF pulse turned off. For comparing contrast-to-noise ratio (CNR), short-axis slices were used to reduce partial voluming when segmenting myocardium. Blood-myocardium contrast was computed from single times frames (from late-diastole) as the difference between average LV blood signal and average septal myocardium signal in regions of interest. Noise levels were computed again by taking the standard deviation in images acquired with the RF pulse turned off. Images were acquired in two volunteers.

RESULTS AND DISCUSSION

Nine healthy volunteers (ages 24–42, eight male, one female) were studied. Each volunteer was scanned for roughly 25 min with the goal of acquiring LV function and visualizing right and left coronary anatomy. All nine were scanned at 3T and two were also scanned at 1.5T for the SNR comparison.

Representative 3T real-time images are shown in Fig. 4. Note that while these images show anatomy and vessel segments at single instances, a longer vessel length is observed in the real-time video due to segments passing through the imaging slice in different cardiac phases. Also note that while viewing the video, noise from successive frames is mostly uncorrelated and does temporally average down.

Figure 4a,b shows end-diastolic and end-systolic short axis frames from one volunteer. Note the high blood SNR and excellent blood-myocardium contrast. Left coronaries can also be seen in cross section due to good fat suppression. There is a noticeable signal falloff due to the limited sensitivity of the 5-inch surface coil, but this can be remedied by using a larger coil or a coil array.

Figure 4c–e contains single frames of right coronary arteries from three volunteers. The ability to see such long segments of the RCA with good contrast indicates good fat suppression. The image in Fig. 4d has a small susceptibility "bite" artifact (black arrow), probably due to air trapped above the liver. Off-resonance is highly nonlinear near the artifact, which could not be corrected with a low-resolution field map. In this case, spins in that area are actually outside the pass-band of the spectral-spatial excitation and can be visualized by shifting the transmit center frequency on the real-time interface (image not shown). Note also that because imaging is performed in real time and each frame is completely acquired in 120 ms, visualization during systole is possible.

Figure 4f–h contains images of left coronary trees in the LAO caudal view. Again, these are single frames from real-time videos and show good image quality for real-time imaging (7). In these views muscle suppression is critical and may be improved by using higher flip angles and sharper slice profiles to saturate the relatively static muscle. Also, these views are far from the surface coil and will benefit the most from better receive coil arrangements.

Two subjects were scanned at both 1.5T and 3T using comparable imaging sequences for an SNR and CNR comparison (parameters in Table 1). Blood SNR was measured in the axial slices shown in Fig. 5a. The signal regions

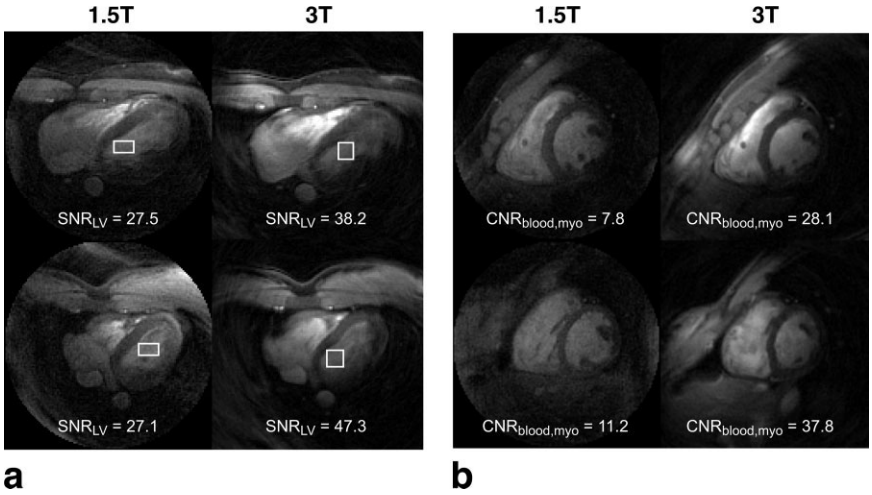

FIG. 5. SNR comparison between 1.5T and 3T. Real-time images from the same volunteer scanned at 1.5T and 3T on consecutive days. Coil position was identical and scan parameters are summarized in Table 1. **a**: SNR_{LV} was measured in axial slices from mid-systole by dividing the average signal in the LV blood pool by the standard deviation of pixel magnitudes with the excitation pulse turned off. The regions used are indicated by the white boxes. A 57% improvement in SNR was observed, which translates to a 53% improvement in SNR efficiency. **b**: CNR between blood and myocardium was measured in short-axis slices from late-diastole. The difference between average LV blood signal and average septal myocardium signal was divided by the standard deviation of pixel magnitudes with the excitation pulse turned off. A CNR improvement of 249% was observed.

(indicated by white boxes) were chosen to encompass as much LV blood pool as possible without including papillaries. A mean blood SNR improvement of 57% was observed, which translates to a 53% improvement in SNR efficiency when considering the different acquisition times. There are several other factors that could affect this comparison, such as scanner calibration, coil positioning, coil tuning, and flip angle and TR differences. In addition, the receive sensitivity of 5-inch surface coils is different at different field strengths. We therefore consider this to be an estimate of the SNR improvement. CNR between blood and myocardium was measured in the short-axis slices shown in Fig. 5b. A blood-myocardium CNR improvement of 249% was observed, which translates to a 232% improvement in CNR efficiency. The drastic CNR improvement can be attributed to the fact that a shorter TR was used at 3T and T_1 relaxation times are longer, resulting in greater saturation of the myocardium during continuous imaging. Reduced myocardium signal, in combination with higher blood signal, produces excellent contrast between the blood and myocardium. Figure 6 contains illustrative real-time coronary images from the two volunteers at both field strengths. The adequate fat suppression and improved SNR, CNR, and image quality can be seen at 3T. With comparable scan parameters, both the qualitative and quantitative improvements at 3T are readily apparent.

CONCLUSIONS

We have implemented and demonstrated real-time cardiac imaging at 3T using a commercial, whole-body system. By redesigning the pulse sequence with shortened excitation and readout, an estimated 53% increase in blood SNR efficiency and 232% increase in blood-myocardium CNR efficiency (compared with 1.5T) was achieved, with reasonable management of susceptibility effects. Real-time cardiac imaging at 3T is feasible and is advantageous due to the increased SNR and CNR.

ACKNOWLEDGMENTS

The authors thank GE Medical Systems-Applied Sciences Lab West for providing 3T scan time for this work. We also thank Drs. Bob Hu, Dwight Nishimura, Jean Brittain, Phillip Yang, Girish Narayan, and Patricia Nguyen for useful discussions and collaboration.

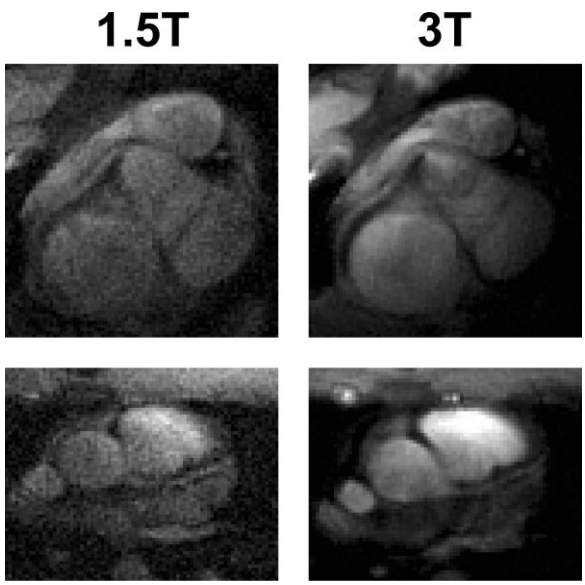

FIG. 6. Real-time coronary images acquired at 1.5T and 3T: (top) right coronary artery and (bottom) left main coronary artery from two different volunteers. Notice the SNR and image quality improvement at 3T.

REFERENCES

1. Kerr AB, Pauly JM, Hu BS, Li KCP, Hardy CJ, Meyer CH, Macovski A, Nishimura DG. Real-time interactive MRI on a conventional scanner. Magn Reson Med 1997;38:355–367.
2. Yang PC, Kerr AB, Liu AC, Liang DH, Hardy CJ, Meyer CH, Macovski A, Pauly JM, Hu BS. New real-time interactive magnetic resonance imaging complements echo cardiography. J Am Coll Cardiol 1998;32:2049–2056.
3. Nagel E, Schneider U, Schalla S, Ibrahim T, Schnackenburg B, Bomstedt A, Klein C, Lehmkuhl HB, Fleck E. Magnetic resonance real-time imaging for the evaluation of left ventricular function. J Cardiovasc Magn Reson 2000;2:7–14.
4. Kaji S, Yang PC, Kerr AB, Tang WH, Meyer CH, Macovski A, Pauly JM, Nishimura DG, Hu BS. Rapid evaluation of left ventricular volume and mass without breath-holding using real-time interactive cardiac magnetic resonance imaging system. J Am Coll Cardiol 2001;38:527–533.
5. Nayak KS, Pauly JM, Kerr AB, Hu BS, Nishimura DG. Real-time color flow MRI. Magn Reson Med 2000;43:251–258.
6. Meyer CH, Hu BS, Kerr AB, Sachs TS, Pauly JM, Macovski A, Nishimura DG. High-resolution multislice spiral coronary angiography with real-time interactive localization. In: Proc 5th Annual Meeting ISMRM, Vancouver, 1997. p 439.
7. Nayak KS, Pauly JM, Yang PC, Hu BS, Meyer CH, Nishimura DG. Real-time interactive coronary MRA. Magn Reson Med 2001;46:430–435.
8. Noeske R, Siefert F, Rhein KH, Rinneberg H. Human cardiac imaging at 3T using phased-array coils. Magn Reson Med 2000;44:978–982.
9. Reeder SB, Faranesh AZ, Boxerman JL, McVeigh ER. In vivo measurement of T_2 and field inhomogeneity maps in the human heart at 1.5T. Magn Reson Med 1998;39:988–998.
10. Singerman RW, Denison TJ, Wen H, Balaban RS. Simulation of B_1 field distribution and intrinsic signal-to-noise in cardiac MRI as a function of static magnetic field. J Magn Reson 1997;125:72–83.
11. Meyer CH, Pauly JM, Macovski A, Nishimura DG. Simultaneous spatial and spectral selective excitation. Magn Reson Med 1990;15:287–304.
12. Schick F. Simultaneous highly selective MR water and fat imaging using a simple new type of spectral-spatial excitation. Magn Reson Med 1998;20:194–202.
13. Zur Y. Design of improved spectral-spatial pulses for routine clinical use. Magn Reson Med 2000;43:410–420.
14. Fredrickson JO, Meyer CH, Pelc NJ. Flow effects of spectral spatial excitation. In: Proc 5th Annual Meeting ISMRM, Vancouver, 1997. p 113.
15. Conolly S, Nishimura DG, Macovski A, Glover G. Variable-rate selective excitation. J Magn Reson 1988;78:440–458.
16. Meyer CH, Pauly JM, Macovski A. A rapid, graphical method for optimal spiral gradient design. In: Proc 4th Annual Meeting ISMRM, New York, 1996. p 392.
17. King KF, Foo TKF, Crawford CR. Optimized gradient waveforms for spiral scanning. Magn Reson Med 1995;34:156–160.
18. Santos JM, Wright G, Yang PC, Pauly JM. Adaptive architecture for real-time imaging systems. In: Proc 10th Annual Meeting ISMRM, Honolulu, 2002. p 468.
19. Jackson JI, Meyer CH, Nishimura DG, Macovski A. Selection of a convolution function for Fourier inversion using gridding. IEEE Trans Med Imag 1991;10:473–478.
20. O'Sullivan JD. A fast sinc function gridding algorithm for Fourier inversion in computer tomography. IEEE Trans Med Imag 1985;4:200–207.
21. Riederer SJ, Tasciyan T, Farzaneh F, Lee IN, Wright RC, Herfkens RJ. MR fluoroscopy: technical feasibility. Magn Reson Med 1988;8:1–15.